Nonrelativistic numerical study of atomic ionization by strong laser fields without the dipole approximation in a flat-atom model

J. R. Vázquez de Aldana and Luis Roso
Departamento de Física Aplicada, Universidad de Salamanca, E-37008 Salamanca, Spain
(Received 28 September 1999; published 2 March 2000)

Numerical experiments for a two-dimensional hydrogen model interacting with very intense (far beyond the barrier suppression value) and linearly polarized laser fields are presented in nonrelativistic cases. The Schrödinger equation retaining the space dependence of the fields is solved (nondipole), comparing with results obtained in the standard dipole approximation, in situations where the validity of such an approximation can be questioned.

PACS number(s): 42.50.Hz, 32.80.Fb

I. INTRODUCTION

The interaction of atoms with intense laser fields has been achieved from many points of view in the past two decades. Talking about theoretical studies, the direct numerical resolution of the time-dependent Schrödinger equation for this system is one of the most powerful research techniques. Different models and approximations have been developed in order to simplify the complexity of such a task. In this way, for example, the dipole approximation (the long wavelength of the fields compared to the typical dimension of the atom) is widely accepted when laser parameters are such that the electron dynamic is expected to be nonrelativistic [1–5]. Howeover, very few quantum calculations have been published in this regime taking into account the spatial dependence of the fields [6,7], testing the dipole approximation. In relativistic situations the nonvalidity of this approximation was clearly shown in different works [8,9].

In this paper we present numerical simulations of a two-dimensional atomic model interacting with very intense (far beyond the barrier suppression) and high-frequency laser fields, solving the Schrödinger equation with the space dependence of the fields retained (nondipole equation), so as the standard dipole Schrödinger equation. Results obtained from both equations are compared, showing the very different behaviors of the atomic electrons in some situations. Laser fields are always linearly polarized in this paper.

In Sec. II the two-dimensional atomic model is introduced and justified for this kind of numerical experiments. The selected geometry in the numerical experiments is also mentioned. The numerical method employed to solve the Schrödinger equation, and details of the calculation, are explained in Sec. III. The effect of the magnetic field is studied in Sec. IV, and other short-wavelength effects are discused in Sec. V. Finally, Sec. VI is devoted to conclusions.

II. FLAT-ATOM HYDROGEN MODEL

Computational requirements to solve the fully three-dimensional time-dependent Schrödinger equation for an atom are extremely prohibitive when the interaction with very intense laser fields is studied. The very large grids that have to be employed in order to avoid reflections and boundary effects make the problem suitable only with massive parallel computers. The dipole approximation in the time-dependent Schrödinger equation allows one to reduce the dimensionality of the problem, thanks to the cylindrical symmetry in the case of a linearly polarized laser field, and many calculations have been done in this way in past years. However, in cases where the dipole approximation is not valid (for example, when magnetic effects are thought to be important) the dimensionality of the problem cannot be directly reduced because the cylindrical symmetry breaks, and a fully three-dimensional treatment has to be employed.

On the other hand, two-dimensional atomic models are very useful because they make it possible to take into account electric and magnetic effects, such as elliptic polarization of the electric field, and are not so prohibitively computation demanding. Moreover two-dimensional models are reasonably realistic, especially if a soft core (smoothed) potential is used which avoids the singularity at the origin:

$$V(x,y) = -\frac{1}{\sqrt{x^2+y^2+a}}. \tag{1}$$

a, the smoothness parameter, has been selected to be $a=1$ a.u. ($\simeq 0.053$ nm). Atomic units ($e=m=\hbar=1$ a.u. and $c=137$ a.u.) are used throughout this paper. The time-independent Schrödinger equation for the atomic model in Cartesian coordinates is

$$-\frac{1}{2}\left(\frac{\partial^2}{\partial x^2}+\frac{\partial^2}{\partial y^2}\right)\Psi(x,y) - \frac{1}{\sqrt{x^2+y^2+1}}\Psi(x,y) = E_B\Psi(x,y). \tag{2}$$

Changing to polar coordinates, $x=\rho\cos(\theta)$, and $y=\rho\sin(\theta)$ Eq. (2) is separable into

$$-\frac{d^2}{d\theta^2}\xi(\theta) = \lambda^2\xi(\theta) \tag{3}$$

$$-\frac{1}{2}\left(\frac{d^2}{d\rho^2}+\frac{1}{\rho}\frac{d}{d\rho}-\frac{\lambda^2}{\rho^2}\right)\phi(\rho) - \frac{1}{\sqrt{\rho^2+a}}\phi(\rho) = E_B\phi(\rho), \tag{4}$$

where $\Psi(\rho,\theta)=\phi(\rho)\xi(\theta)$. The equation for the polar angle [Eq. (3)] is trivially solved: $\xi(\theta)=e^{i\lambda\theta}$, with $\lambda=0,\pm1,\pm2,\ldots$. The radial equation [Eq. (4)] can be easily integrated numerically with standard one-dimensional methods (that of Numerov, for example). In order to solve the time-dependent Schrödinger equation of an atom interacting with laser fields, it is convenient to use a grid in Cartesian coordinates (equally separated points along axes x and y) because we thus obtain a uniform sampling of all the integration surface. To calculate eigenfunctions in a two-dimensional Cartesian grid is not as easy as in one-dimensional problems, and more sophisticated methods have to be employed (see Sec. III), because eigenstates of the radial equation [Eq. (4)] are not exactly the same as those of the Cartesian equation.

In the simulations presented in this paper, the electric field is linearly polarized in the y direction, and the pulse propagates along the x direction:

$$\vec{E}(x,t)=E_0 f(x,t)\sin(kx-\omega_L t)\vec{e}_y. \tag{5}$$

$f(x,t)$ is the laser pulse turn-on. In the calculations presented in this paper we have selected a linear turn-on (that lasts four cycles of the electromagnetic fields) because it does not introduce the well-known drift along the polarization axis.

Then the vector potential and the magnetic field are

$$\vec{A}(x,t)=-c\int_0^t E(x,t')dt'\vec{e}_y,$$
$$\vec{B}(x,t)=\vec{\nabla}\times\vec{A}(x,t)=B(x,t)\vec{e}_z, \tag{6}$$

with a convenient choice of gauge where the scalar potential is taken to be zero. The vector potential is polarized in the same direction as the electric field, and the magnetic field is parallel to the z axis (perpendicular to the flat-atom plane). Neglecting the atomic potential, the motion of a free nonrelativistic electron in these electromagnetic fields is given by the Lorentz equation

$$\frac{d^2\vec{r}}{dt^2}=-\left(E(x,t)\vec{e}_y+\frac{1}{c}\vec{v}\times\vec{B}(x,t)\right), \tag{7}$$

and splitting it into components:

$$\frac{d^2x}{dt^2}=-\frac{1}{c}v_y B(x,t),$$
$$\frac{d^2y}{dt^2}=-E(x,t)+\frac{1}{c}v_x B(x,t), \tag{8}$$
$$\frac{d^2z}{dt^2}=0.$$

Then the classic Lorentz force causes the electron motion to be confined in the xy plane (if it is initially at rest, or at least, has no velocity in the z direction), making the present two-dimensional model reasonably realistic because the motion is by itself included in this plane.

In that case, the nondipole Schrödinger equation is

$$i\frac{\partial}{\partial t}\Psi(x,y,t)=\left[-\frac{1}{2}\left(\frac{\partial^2}{\partial x^2}+\frac{\partial^2}{\partial y^2}\right)-\frac{i}{c}A(x,t)\frac{\partial}{\partial y}+\frac{1}{2c^2}A(x,t)^2+V(x,y)\right]\Psi(x,y,t), \tag{9}$$

where obviously the spatial dependence of the fields has been retained. When the dipole approximation can be assumed, that is $A(x,t)\simeq A(t)$, Eq. (9) reduces to

$$i\frac{\partial}{\partial t}\Psi(x,y,t)=\left[-\frac{1}{2}\left(\frac{\partial^2}{\partial x^2}+\frac{\partial^2}{\partial y^2}\right)-\frac{i}{c}A(t)\frac{\partial}{\partial y}+V(x,y)\right]\Psi(x,y,t) \tag{10}$$

(eliminating the ponderomotive term with a time-dependent phase), which is the standard time-dependent dipole Schrödinger equation in the velocity gauge ($\vec{p}\cdot\vec{A}$). It is well known that the length gauge ($\vec{E}\cdot\vec{r}$) has no meaning when working out of the dipole approximation, because it is not possible to separate space and momentum coordinates in the coupling term $-(i/c)A(x,t)(\partial/\partial y)$. Then it has to be solved with no transformation.

III. NUMERICAL RESOLUTION

Numerical resolution of the time-dependent dipole Schrödinger equation has been carried out extensively in the past two decades, and thus, very sophisticated techniques have been developed (see, for example Ref. [4], and references therein). In general, for a given time-dependent Schrödinger-like equation,

$$i\frac{\partial}{\partial t}\Phi(x,y,t)=\hat{H}(x,y,t)\Phi(x,y,t); \tag{11}$$

knowing the wave function at a time t, it is possible to formally calculate it in the time step $t+\Delta t$ as

$$\Phi(x,y,t+\Delta t)=\exp\left[-i\int_t^{t+\Delta t}\hat{H}(x,y,t')dt'\right]\Phi(x,y,t)$$
$$\simeq\exp\left[-i\Delta t\hat{H}\left(x,y,t+\frac{\Delta t}{2}\right)\right]\Phi(x,y,t). \tag{12}$$

This is the starting point for most of the numerical methods. Now we split the exponential into three terms [10]:

$$\Phi(x,y,t+\Delta t)\simeq\exp\left[-\frac{i\Delta t}{2}\hat{H}_x\left(x,y,t+\frac{\Delta t}{2}\right)\right]\times\exp\left[-i\Delta t\hat{H}_y\left(x,y,t+\frac{\Delta t}{2}\right)\right]\times\exp\left[-\frac{i\Delta t}{2}\hat{H}_x\left(x,y,t+\frac{\Delta t}{2}\right)\right]\times\Phi(x,y,t)+O(\Delta t^3). \quad (13)$$

In general, the operators $\hat{H}_x$ and $\hat{H}_y$ do not conmute themselves, and that is the reason why this expression is not an equality: it is exact to the order Δt^2.

The Hamiltonian operators $\hat{H}_x(x,y,t)$ and $\hat{H}_y(x,y,t)$ are different in the case of the dipole Schrödinger equation than in the nondipole equation. In order to solve Eq. (10), we have chosen

$$\hat{H}_x(x,y,t)=-\frac{1}{2}\frac{\partial^2}{\partial x^2}+\frac{1}{2}V(x,y),$$
$$\hat{H}_y(x,y,t)=-\frac{1}{2}\frac{\partial^2}{\partial y^2}+\frac{1}{2}V(x,y)-\frac{i}{c}A(t)\frac{\partial}{\partial y}, \quad (14)$$

and, in the case of the nondipole Schrödinger equation [Eq. (9)],

$$\hat{H}_x(x,y,t)=-\frac{1}{2}\frac{\partial^2}{\partial x^2}+\frac{1}{2}V(x,y)+\frac{1}{2c^2}A(x,t)^2,$$
$$\hat{H}_y(x,y,t)=-\frac{1}{2}\frac{\partial^2}{\partial y^2}+\frac{1}{2}V(x,y)-\frac{i}{c}A(x,t)\frac{\partial}{\partial y}. \quad (15)$$

Each time step, Eq. (13) is solved, employing the Cayley-Hamilton form and a Crank-Nicholson finite-difference scheme. The widely used methods that solve Eq. (13), by means of a Fourier transform, cannot be directly implemented in the case of the nondipole Schrödinger equation, because the term

$$-\frac{i}{c}A(x,t)\frac{\partial}{\partial y} \quad (16)$$

mixes space and momentum coordinates, and it is not possible to separate them. Of course, a combined method employing Fourier-transform and Crank-Nicholson schemes is also suitable.

The initial state in the grid has been calculated by means of the imaginary-time propagation method. A function in the grid is chosen (as similar as possible to the ground state), and it is made to evolve in time with an imaginary time step: $t_0 \rightarrow t_0+i\Delta t$. Numerical algorithms for this purpose are the same as those used in calculating the time evolution of the Schrödinger wave function, changing Δt by $i\Delta t$. This technique allows one to determine not only the ground state of the model but also a few low-lying states, by imposing orthogonallity with the lower-energy states that have been previously calculated.

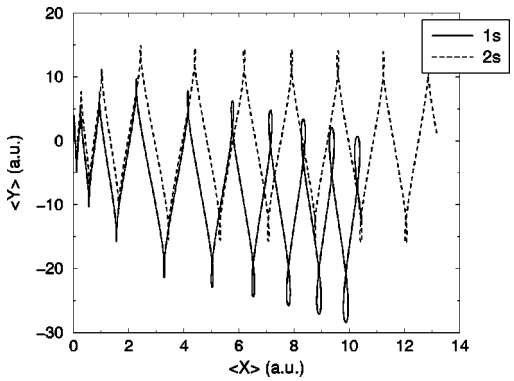

FIG. 1. Expected value of the wave-packet trajectory (nondipole equation), for the initial states $1s$ (solid line) and $2s$ (dashed line), in atomic units. Laser parameters are $E_0=15$ a.u. ($I\simeq 7.9\times10^{18}$ W/cm^2) and frequency $\omega_L=1$ a.u. ($\simeq$27.2 eV). The linear turn-on of the laser lasts four cycles of the electric field.

For the selected smoothing parameter value in this paper $a=1$ a.u. ($\simeq$0.053 nm), and, employing a Cartesian grid of 1000×1000 points with spatial separation between two consecutive points $\Delta x=\Delta y=0.05$ a.u. ($\simeq$0.0027 nm), the

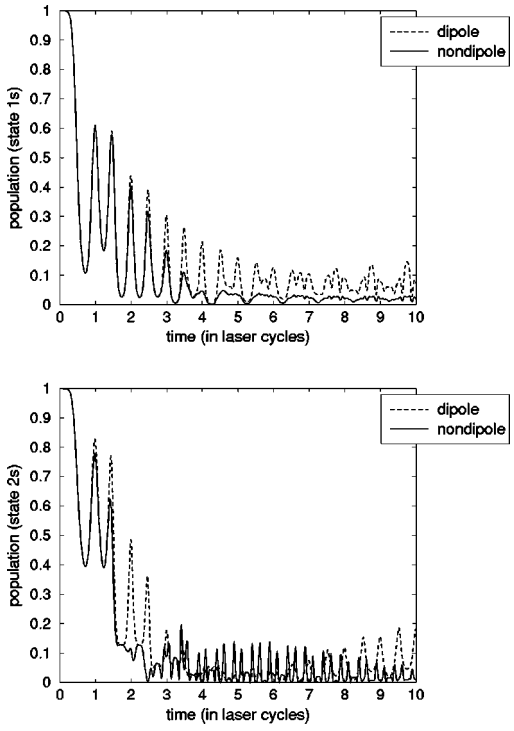

FIG. 2. Time evolution of the population that remains in the initial state, comparing between results obtained in the dipole approximation (dashed line) and without this approximation (solid line). In the plot at the top, the initial state of the model is $1s$, and in the plot at the bottom it is $2s$. Laser parameters are $E_0=15$ a.u. ($I\simeq7.9\times10^{18}$ W/cm^2) and frequency $\omega_L=1$ a.u. ($\simeq$27.2 eV). The linear turn-on of the laser lasts four cycles of the electric field.

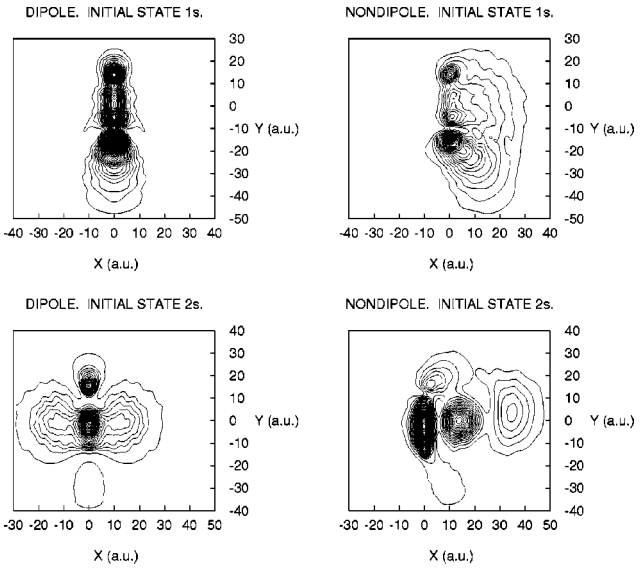

FIG. 3. Contour plots of the probability density $|\Psi(x,y,t)|^2$ after ten cycles of the field (the same parameters as in the Fig. 2). Graphics at the top correspond to an initial state taken to be $1s$, and that at the bottom to a state taken to be $2s$. The column at the left shows the dipole case, and the one at the right in the nondipole integration. The linear scale of the contour levels is the same for all the plots.

ground state energy of the two-dimensional atom model is $E(1s)=-0.43$ a.u. ($\simeq -11.7$ eV). $2s$ and $2p$ states have an energy in this grid of $E(2s)=-0.12$ a.u. ($\simeq -3.3$ eV). The evolution of $1s$ and $2s$ states is studied in this paper. We have used different grids to solve the Schrödinger equation, depending on the classic excursion of the electron, as is explained in each case.

IV. MAGNETIC-FIELD DRIFT

As we have seen above, the dipole approximation neglects the magnetic field because it assumes that the vector potential is not space dependent [Eqs. (6)]. When the interaction of an electron with linearly-polarized lasers is classically studied [the nonrelativistic Lorentz equation, Eq. (7)] in this approximation, the electron motion is restricted to the polarization direction. The velocity oscillates with amplitude $v_0=E_0/\omega_L$. As this classic velocity increases ($v_0 \geqslant 0.1c$), magnetic-field effects appear, and the dipole approximation can be seriously questioned; even though the laser wavelength was very large compared to typical atomic dimensions, $\lambda \gg \langle r \rangle_{nl}$. These effects have sometimes been called relativistic effects, because they are more important for high electron velocities, but they can also be observed in nonrelativistic equations. In fact, such an effect appears in the second term in Eq. (7).

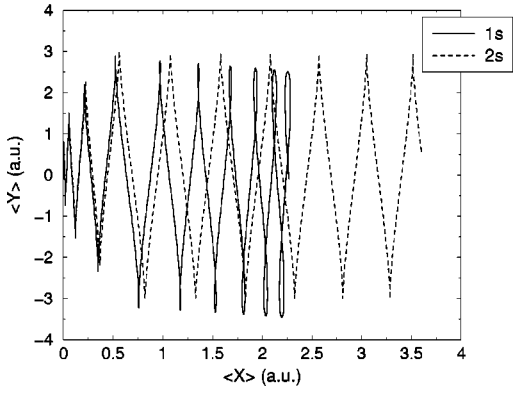

FIG. 4. Expected value of the wave-packet trajectory (nondipole equation) for the initial $1s$ (solid line) and $2s$ (dashed line) states, in atomic units. Laser parameters are $E_0=75$ a.u. ($I\simeq 2.0\times 10^{20}$ W/cm^2) and frequency $\omega_L=5$ a.u. ($\simeq 136.1$ eV). The linear turn-on of the laser lasts four cycles of the electric field.

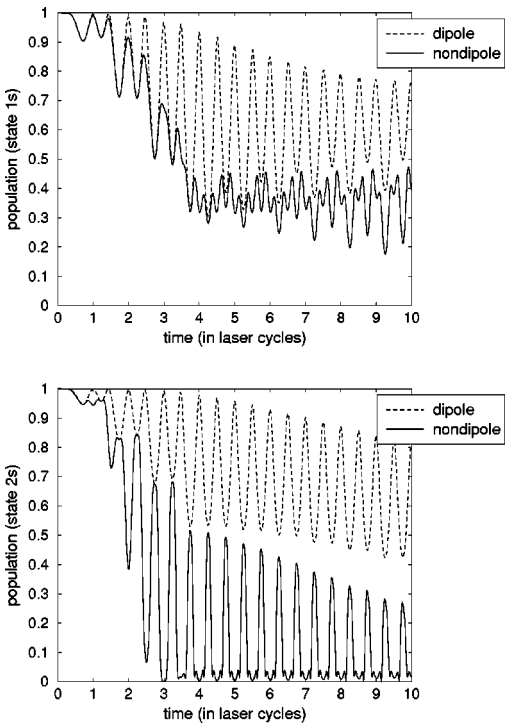

FIG. 5. Time evolution of the population that remains in the initial state, comparing between results obtained in the dipole approximation (dashed line) and without this approximation (solid line). In the plot at the top, the initial state of the model is $1s$, and in the plot at the bottom it is $2s$. Laser parameters are $E_0=75$ a.u. ($I\simeq 2.0\times 10^{20}$ W/cm^2) and frequency $\omega_L=5$ a.u. ($\simeq 136.1$ eV). The linear turn-on of the laser lasts four cycles of the electric field.

The main effect of the magnetic field in the electron motion [11] is a drift along the propagation direction (x in this paper). This can also be understood as momentum transferred to the electrons by the incident photons. For a given value of the classic velocity v_0, this effect is more important as the classical excursion of the electron $\alpha_0=E_0/\omega_L^2$ increases.

An estimation of the magnitude of the magnetic-field drift for an initially at rest free electron can be easily done by neglecting the spatial dependence of the fields in Eq. (7). In the case of a squared pulse (for simplicity), the electron moves along the propagation axis with constant speed in addition to oscillatory terms. This velocity is approximately

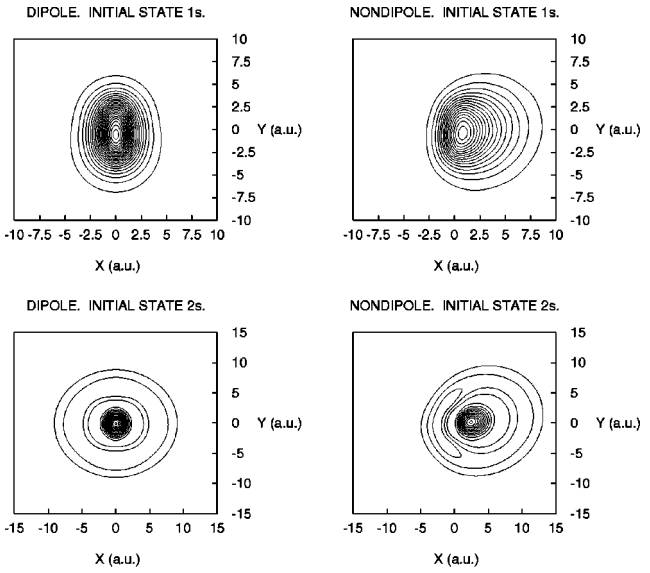

FIG. 6. Contour plots of the probability density $|\Psi(x,y,t)|^2$ after ten cycles of the field (the same parameters as in Fig. 5). Graphics at the top correspond to the initial state taken to be $1s$, and that at the bottom to be $2s$. The column at the left shows the dipole case, and the one at the right the nondipole integration. The linear scale of the contour levels is the same for all the plots.

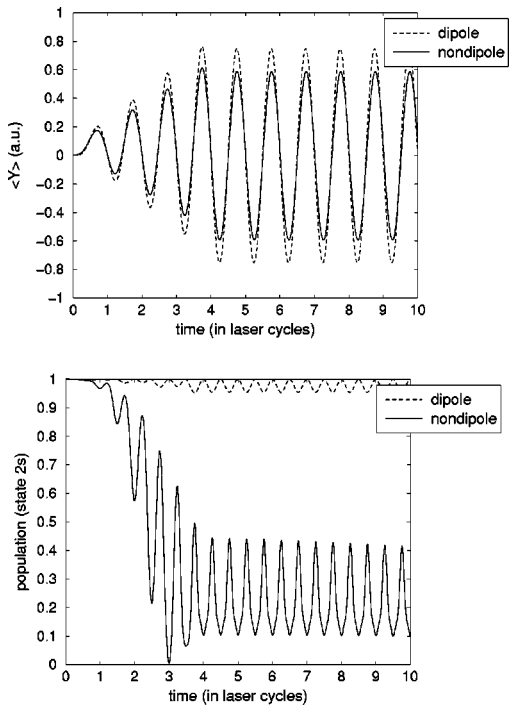

FIG. 7. Expected value of the wave-packet motion along the polarization direction for the initial states $2s$, in dipole (dashed line) and nondipole (solid line) integrations. In the plot at the bottom, we show the time evolution of the population of this state in dipole (dashed line) and nondipole (solid line) integrations. Laser parameters are $\omega_L=20$ a.u. ($\simeq 544$ eV) and $E_0=300$ a.u. ($I\simeq 3.2\times 10^{21}$ W/cm^2).

$v_{drift}\simeq 3E_0^2/(4c\omega_L^2)$. The displacement in this direction is then $x_{drift}\propto E_0^2 t/(c\omega_L^2)$. Thus, the longer the interaction time, the larger that effect.

Figures 1, 2, and 3 show the results obtained when interacting with a ten cycle laser pulse of amplitude $E_0=15$ a.u. ($I\simeq 7.9\times 10^{18}$ W/cm^2) and frequency $\omega_L=1$ a.u. ($\simeq 27.2$ eV). The linear turn-on of the laser lasts four cycles of the electric field. We have employed a spatial grid with 3000×1300 points, equally separated $\Delta x=\Delta y=0.2$ a.u. ($\simeq 0.01$ nm). In Fig. 1 we plot the expected value of the wave-packet trajectory, that is $\langle\vec{r}\rangle=\int\Psi(x,y,t)\vec{r}\Psi(x,y,t)^*dxdy$, for two different initial states: the ground $1s$ state (solid line) and the $2s$ state (dashed line) of the two-dimensional model. The magnetic-field drift is very important, and leads to a displacement in the x direction of the same order of magnitude (after ten cycles) as the motion along the polarization axis. The classic velocity in this case is $v_0=E_0/\omega_L=15$ a.u., and the estimated drift velocity is $v_{drift}\simeq 1.2$ a.u. (a displacement of 75 a.u. after ten cycles). Of course, this estimation is too large compared to numerical results, but the discrepancies are well explained because in the estimation we have neither taken the laser turn-on into account nor the Coulomb potential. Both effects decrease the magnitude of this motion. The irregular behavior of the $1s$ state is a consequence of the fact that this state has a smaller energy than the $2s$ state, and it interacts more strongly with the Coulomb potential. Figure 2 shows the time evolution of the initial state population ($1s$ and $2s$ states, up and down, respectively), comparing results obtained with the dipole approximation and with the nondipole Schrödinger equation. It is clearly seen in the $1s$ case that this state loses more population in the nondipole calculation because of the magnetic drift. This is not so evident in the $2s$ time evolution because of the particular shape of such a state. Figure 3 shows the contour plots of the probability density $|\Psi(x,y,t)|^2$ after the interaction time. The scale of the contour lines is linear, and it is the same for all the plots. It is important to realize that the axial symmetry along the polarization direction in the dipole approximation strongly breaks when taking into account the spatial dependence of the fields. The population spreads not only in this direction as predicted by stabilization theories, but also in the propagation direction.

Figures 4, 5, and 6, show the same plots as the previous figures, but now we study the interaction with a ten-cycles laser pulse of amplitude $E_0=75$ a.u. ($I\simeq 2.0\times 10^{20}$ W/cm^2) and frequency $\omega_L=5$ a.u. ($\simeq 136.1$ eV). The linear turn-on of the laser lasts four cycles. The grid that we have employed now has 3000×1000 points, equally separated by $\Delta x=\Delta y=0.05$ a.u. ($\simeq 0.0027$ nm). The different behavior between dipole and nondipole integration, mainly for the $2s$ state in Fig. 5, is more evident than in the previous case, because the motion along the propagation axis is now as important as the oscillations in the polarization axis. Now the wave functions distort just a little because the interaction time is very short, and natural spreading of the wave function is negligible (Fig. 6). That is the reason why wave packets maintain more or less their original shape.

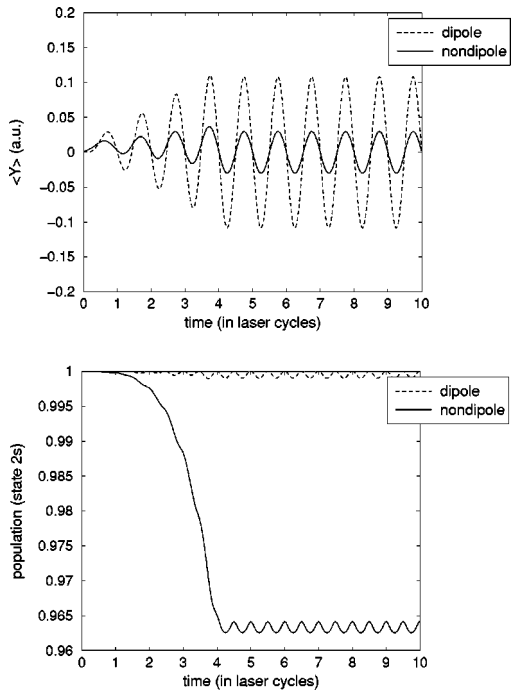

FIG. 8. Expected value of the wave-packet motion along the polarization direction for the initial states $2s$, in dipole (dashed line) and nondipole (solid line) integrations. In the plot at the bottom, we show the time evolution of the population of this state in dipole (dashed line) and nondipole (solid line) integrations. Laser parameters are $\omega_L=43$ a.u. ($\simeq 1.17$ keV) and amplitude $E_0=200$ a.u. ($I\simeq 1.4\times 10^{21}$ W/cm^2).

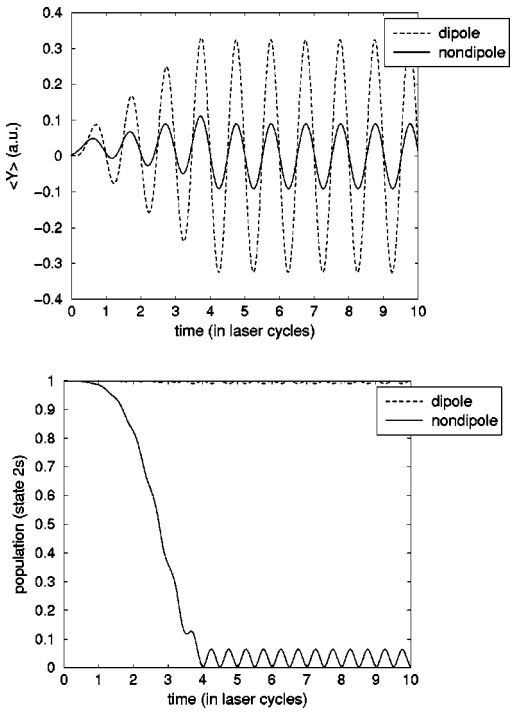

FIG. 9. Expected value of the wave-packet motion along the polarization direction for the initial states $2s$, in dipole (dotted line) and nondipole (solid line) integrations. In the plot at the bottom, we show the time evolution of the population of this state in dipole (dotted line) and nondipole (solid line) integrations. Laser parameters are $\omega_L=43$ a.u. ($\simeq 1.17$ keV) and amplitude $E_0=600$ a.u. ($I\simeq 1.3\times 10^{22}$ W/cm^2).

V. SHORT-WAVELENGTH EFFECTS

In cases where the laser wavelength is comparable to the size of the atomic state that we are considering, the dipole approximation is clearly not valid, and does not depend on the electronic velocity and its coupling with the magnetic field. As the electric field varies significantly along the propagation axis (x), each ''line'' of the atomic wave function perpendicular to this axis experiences a different value of the electric and magnetic fields at the same time. So the wave function is expected to behave in a very different way than in cases where the whole wave function is affected by a uniform electric field.

If we study the hydrogen $1s$ state, whose dimension is tvpically of the order of 1 a.u. ($\simeq 0.053$ nm), the required laser frequency to find this effect [more than $\omega_L \simeq 150$ a.u. ($\simeq 4.1$ KeV)] is clearly unrealistic for the lasers available nowadays. However, it is possible to consider highly excited states (Rydberg states) which have a very large spatial extension so that, with lasers in the visible range, the dipole approximation is again questioned. For example, the $n=40$ Rydberg state has a spatial dimension comparable with a wavelength of $\lambda=500$ nm (visible).

In this paper, we present some calculations starting from the $2s$ state of the flat-atom model, which has a spatial extension of approximately 10 a.u. ($\simeq 0.53$ nm) larger than the size of the state $1s$. The grid that we have employed has 1000×1000 points, equally separated $\Delta x=\Delta y=0.05$ a.u. ($\simeq 0.0027$ nm).

In Fig. 7, we show the time evolution of the expected value of the y coordinate (the polarization direction), and the population of the selected initial state. Laser parameters are $\omega_L=20$ a.u. ($\simeq 544$ eV) and $E_0=300$ a.u. ($I\simeq 3.2\times 10^{21}$ W/cm^2). The laser turn-on is again linear, and it lasts four cycles of the electric field. The amplitude of the oscillations along the polarization axis is smaller in the nondipole case than in the dipole one. This effect is caused by the strong spatial dependence of the electric field, that does not move the wave function as a whole, but each line perpendicular to the x axis, in a different way. So, on average, the motion of the wave packet is smaller than expected in the dipole approximation. The wave packet becomes deformed, instead of oscillating. It can be said that each point of the wave function moves classically, and independent of the remaining population.

The population of the state evolves surprisingly different in both cases. In the dipole approximation result, population oscillates as one would expect from the small sinusoidal motion shown in the graphic above. The wave packet moves freely with no distortion, taking into account that the frequency of the field is very large (the interaction time is small) and that the natural spread of the wave function is negligible. However, in the nondipole calculation the $2s$ state loses most of its population in a few cycles of the field. This is caused by a local phase shift induced by the field in the wave function [12], which is esentially the classical action for each point of the wave packet, that depends on the x

coordinate. Even though the population remains near the nucleus (very small oscillations of the wave packet), the overlapping of the evolved wave function and the initial wave function is very small because this phase destructively interferes when evaluating the population.

Figures 8 and 9 show the same magnitudes as in Fig. 7, but now the frequency of the laser is $\omega_L = 43$ a.u. ($\simeq 1.17$ keV), and the amplitude $E_0 = 200$ a.u. ($I \simeq 1.4 \times 10^{21}$ W/cm^2) and $E_0 = 600$ a.u. ($I \simeq 1.3 \times 10^{22}$ W/cm^2), respectively. The short-wavelength effects studied above, now become more evident because of the frequency selected for the calculation, that causes a change of π in the phase of the fields in the spatial region occupied by the electronic wave packet. The effect of the laser amplitude can be observed by comparing between Figs. 8 and 9 for the same value of the frequency.

VI. CONCLUSIONS

In this paper we have solved the time-dependent Schrödinger equation, mantaining the whole spatial dependence of the electric and magnetic fields (the nondipole Schrödinger equation). With the very intense lasers available nowadays, it is possible to find situations for which the standard dipole approximation cannot be assumed, and the Schrödiger equation has to be solved with no approximations. We have pointed out two different situations, both of them with over the barrier suppresion and with frequencies over the atomic unit (the photon energy is 27.2 eV).

In the first situation, the electron quiver velocity is high, but not high enough to solve relativistic wave equations ($v_0 = E_0/\omega_L \simeq 10$ a.u.). In this case, the magnetic field cannot be neglected. It leads to a spatial drift of the wave function along the propagation axis, which becomes very important when the classic excursion of the free electron is large ($\alpha_0 = E_0/\omega_L^2$). It can be as important as the oscillatory motion along the polarization direction. Then the very well-studied stabilization and Kramer-Henneberger methods can be questioned. In addition, when the laser wavelength is comparable to the atomic size, $\lambda \simeq \langle r \rangle_{nl}$, the space dependence of the fields cannot be neglected. The effect of this dependence causes a local and semiclassic behavior of each point of the wave function, which differs strongly from the global motion observed in the dipole approximation.

ACKNOWLEDGMENTS

Partial support from the Training and Mobility of Researchers Program of European Commission, from the Spanish Dirección General de Investigación Científica y Técnica (under Contract No. PB95 0955), and from the Consejería de Educación y Cultura of the Junta de Castilla y León (Fondo Social Europeo) under Grant No. SA56/99 are acknowledged.

[1] K.C. Kulander, K.J. Schafer, and J.L. Krause, in *Atoms in Intense Laser Fields*, edited by M. Gavrila (Academic, Boston, 1992).
[2] J.H. Eberly, R. Grobe, C.K. Law, and Q. Su, in *Atoms in Intense Laser Fields* (Ref. [1]).
[3] M. Gavrila (Ref. [1]).
[4] M. Protopapas, C.H. Keitel, and P.L. Knightl, Rep. Prog. Phys. **60**, 389 (1997).
[5] A. Patel, N.J. Kylstra, and P.L. Knight, Opt. Express **4**, 496 (1999).
[6] O. Latinne, C.J. Joachain, and M. Drr, Europhys. Lett. **26**, 333 (1994).
[7] A. Bugacov, M. Pont, and R. Shakeshaft, Phys. Rev. A **48**, R4027 (1993).
[8] T. Katsonleas and W.B. Mori, Phys. Rev. Lett. **70**, 1561 (1993).
[9] C.H. Keitel and P.L. Knight, Phys. Rev. A **51**, 1420 (1995).
[10] A.D. Bandrauk and H. Shen, J. Chem. Phys. **99**, 1185 (1993).
[11] J.R. Vázquez de Aldana and Luis Roso, Opt. Express, **5**, 144 (1999).
[12] J.R. Vázquez de Aldana and Luis Roso (unpublished).